Seed-Induced, Structure Directing Agent-Free Crystallization of Sub-Micrometer Zeolite ZSM-5: A Population Balance Analysis

ARTICLE *in* CRYSTAL GROWTH & DESIGN · MARCH 2012

Impact Factor: 4.89 · DOI: 10.1021/cg200981d

CRYSTAL GROWTH & DESIGN

Article

pubs.acs.org/crystal

Seed-Induced, Structure Directing Agent-Free Crystallization of Sub-Micrometer Zeolite ZSM-5: A Population Balance Analysis

Nan Ren,[†] Josip Bronić,[‡] Tatjana Antonić Jelić,[‡] Ana Palčić,[‡] and Boris Subotić*[,‡]

[†]Department of Chemistry, Shanghai Key Laboratory of Molecular Catalysis and Innovative Materials and Laboratory of Advanced Materials, Fudan University, Shanghai 200433, P. R. China

[‡]Division of Materials Chemistry, Laboratory for the Synthesis of New Materials, Ruđer Bošković Institute, Bijenička 54, 10000 Zagreb, Croatia

Supporting Information

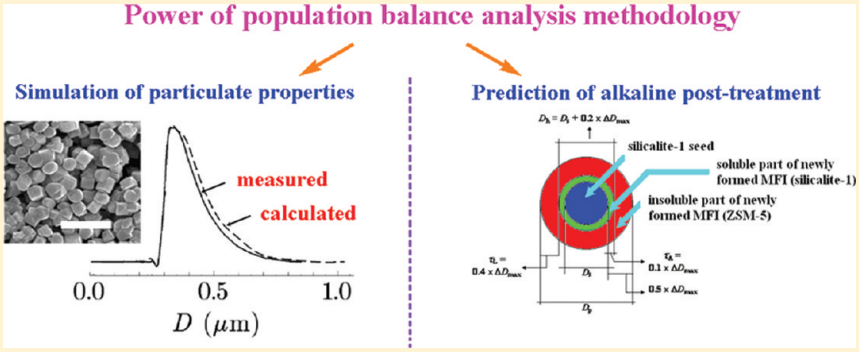

ABSTRACT: Crystallization of sub-micrometer sized zeolite ZSM-5 from a TPA-free (TPA = tetrapropyl ammonium) reaction mixture $1.0Al_2O_3/100SiO_2/28Na_2O/4000H_2O$, seeded with silicalite-1 seed crystals of two different sizes (260 and 690 nm), was analyzed by population balance methodology. Changes in crystal size distributions and fractions of the newly formed crystalline phase (ZSM-5) were measured and compared with the calculated (simulated) data. For the crystalline end products having $D \geq 0.5$ μm (D is the equivalent spherical diameter as measured by a laser-light scattering method), a small disagreement between measured and simulated crystal size distributions is observed and explained by the formation of a small proportion of crystal aggregates at the end of the crystallization process. However, an almost perfect correlation between measured and simulated kinetics of crystallization shows that the formation of aggregates do not considerably influence the growth rate of zeolite ZSM-5 on silicalite-1 seed crystals. Analysis of the obtained results has also shown that the crystallization process takes place only by a linear, size-independent growth of silicalite-1 seed crystals embedded in the gel matrix and thus that the process of crystallization is consistent with the absence of extra nucleation in the presence of seed crystals. Moreover, such methodology was also applied for the analysis of the alkaline-treated products. The obtained results show that the applied population balance methodology enables control and prediction of the particulate properties of as-synthesized and alkaline-treated crystalline end products, which is of great significance for their further applications.

1. INTRODUCTION

Although a variety of different types of zeolites are known,[1] zeolite ZSM-5 is one of the most intensively studied candidates in last 40 years. Such a great and enduring interest for zeolite ZSM-5 was mainly expressed because of its wide and considerable applications (primarily in catalysis and separation) in fuel and petrochemical processing.[2]

It is well established that regardless of the type of zeolite catalyst and the type of catalytic reaction, respectively, the smallest crystals are the most effective ones.[2c,3] With decreasing crystal size, the undesired diffusion limitations of the reactants/intermediates/products can be reduced or even eliminated during the reaction. Such a phenomenon renders the catalysts with high reactivity and long life toward deactivation.[3a,b,4] For this reason, the synthesis and application of small-sized ZSM-5 zeolites in many important catalytic reactions[5] has been recognized as one of the hottest topics in the domain of catalysis and material science.[6]

Zeolite ZSM-5 is conventionally synthesized by hydrothermal treatment of the reactive gel containing aluminosilicate as well as tetrapropylammonium ions (TPA^+) as a structure directing agent (SDA).[2a,7] However, the organic SDAs used in conventional synthesis of ZSM-5 are often poisonous and expensive for massive industrial production. Moreover, the energetic consumption and environmental pollution are also inevitable during removal of these organic species at high temperature.

Received: July 29, 2011
Revised: February 21, 2012
Published: February 22, 2012

   dx.doi.org/10.1021/cg200981d | *Cryst. Growth Des.* 2012, 12, 1736–1745

The difficulties connected with the use of organic SDAs, especially tetrapropylammonim compounds in the synthesis of zeolite ZSM-5, may be eliminated by adoption of TPA^+-free synthesis. Such an approach not only renders calcinations unnecessary but also employs cheaper, less toxic reactants and allows easier waste disposal.[8] However, unlike the case with TPA^+-containing reaction mixtures, the crystallization of zeolite ZSM-5 from TPA^+-free batches often yields impurity phases,[9] different from zeolite ZSM-5. In addition, another concern in the synthesis of zeolite ZSM-5 without an organic template is its large (micrometer sized) and uncontrollable crystal size which significantly influences its catalytic properties.[2d] Finally, the long crystallization time and low yield,[10] respectively, are also big obstacles in industrial production of zeolite ZSM-5 from an organic template-free system.

The above-mentioned disadvantages can be overcome by the addition of a small amount of seed crystals (ZSM-5, silicalite-1) in the TPA^+-free reaction mixture.[2b,10,11] Addition of seed crystals results in the formation of zeolite ZSM-5 with a high degree of crystallinity and a narrow size distribution at short synthesis times.[10,11c]

Taking into consideration technical, economical, and ecological advantages of SDA-free synthesis[8,9a,b,12] and positive effects of seeding on the formation of zeolite ZSM-5 crystals,[10,11] recently we reported a controllable and low-cost procedure for the synthesis of zeolite ZSM-5 with adjustable sub-micrometer crystal size and the specific structure with all-silica core and aluminum-containing shell.[13]

On the other hand, alkaline postsynthesis treatment of as-synthesized ZSM-5 zeolites is a newly developed, very interesting topic. The unusual morphological and textural properties including the generation of controllable mesoporosity and opening of hollow interior endows the material with superior catalytic reactivity compared with its parent counterparts.[14] Besides the useful applications, such kind of research can also elucidate the mechanism of crystallization of zeolite ZSM-5 by clarifying the spatial distribution of Al atoms in the pentasil framework which directly relates to the synthesis conditions.[15]

Among the diverse kinds of secondary ZSM-5 products obtained via alkaline postsynthesis treatment, the hollow particles with the shell of zeolite ZSM-5 receive much interest.[13,14c] Such hollow ZSM-5 particles are expected to be potential high-performance catalysts due to increased surface area and special capsular morphology. Its reactivity is largely determined by the amount, strength, and distribution of active sites located in the ZSM-5 shell. Thus, the prediction and control of both the size of hollow capsules and the thickness of ZSM-5 shell through the control of the crystallization pathway is important for potential applications. Fortunately, the alkaline-treated products from our seed-induced, SDA-free approach bear a hollow nature, which is a good basis for further extensive research. For this reason, based on the proposed mechanism of crystallization,[13] in this work, we created population balance model of crystallization which enables the evaluation of the proposed mechanism and prediction of the particulate properties of both as-synthesized and alkaline-treated products. The kinetics of crystallization and crystal size distribution data simulated (calculated) by the developed model were compared with the corresponding measured data in order to reveal the interesting features of the critical processes which occur during crystallization and alkaline treatment.

2. EXPERIMENTAL SECTION

2.1. Materials. The reagents used for the synthesis and alkaline post-treatment are sodium hydroxide (NaOH, AR, Shanghai Chemical Co. China), tetraethyl orthosilicalite (TEOS, AR, Shanghai Chemical Co. China), tetrapropylammonium hydroxide (TPAOH, 40 wt % aqueous solution AR, Alfa Aesar), colloidal silica suspension (40 wt % of amorphous SiO_2 dispersed in water, Alfa Aesar), aluminum sulfate ($Al_2(SO_4)_3 \cdot 18H_2O$, AR, Shanghai Chemical Co. China), and sodium carbonate (Na_2CO_3, AR, Shanghai Chemical Co. China). Demineralized water was used as solvent. All chemicals were used without any purification.

2.2. Synthesis. The silicalite-1 seed crystals having the sizes 260 nm (s-260) and 690 nm (s-690) were synthesized from "clear solution" approach as follows:[13] TEOS was added into the mixture of TPAOH, NaOH, and water. The obtained reaction mixture ($4.4TPAOH/0.1Na_2O/25SiO_2/xH_2O/100EtOH$; x = 1040 for the seed s-260 and x = 1243 for the seed s-690) was stirred at ambient temperature for 24 h and then transferred to a polypropylene bottle and hydrothermally treated at 100 °C for 1 day. The obtained product (fully crystalline silicalite-1 nanocrystals suspended in the mother liquor) was directly used as the seed suspension, without any centrifugation or washing process.

The reaction mixture, $1.0Al_2O_3/100SiO_2/28Na_2O/4000H_2O$, was prepared by dissolving aluminum sulfate in solution of sodium hydroxide, followed by the addition of colloidal silica solution under stirring. The suspension of silicalite-1 seed crystals was added into the reaction mixture after being stirred for 15 min. The added amount of seed crystals was 4, 8, 16, and/or 32 wt % relative to the total amount of silica in the reaction mixture. No additional amount of TPAOH was added in the starting gel so that the entire amount of the organic template arises only from the added suspension of seed crystals. Such prepared reaction mixtures are denoted as S690-4 (system I: 4 wt % of seeds s-690), S260-4 (system II: 4 wt % of seeds s-260), S260-8 (system III: 8 wt % of seeds s-260), S260-16 (system IV: 16 wt % of seeds s-260) and S260-32 (system V: 32 wt % of seeds s-260). The reaction mixture was further stirred at ambient temperature for 3 h and then divided among needed number of autoclaves. The autoclaves filled with reaction mixture were put into the oven preheated at crystallization temperature (210 °C). The moment when the autoclaves were put into preheated oven was taken as the zero time (t_c = 0) of the crystallization process. At predetermined crystallization times, t_c, the selected autoclaves were taken out from the oven and cooled down to the ambient temperature by tap water. After the autoclave was cooled, the solid phase was separated from the liquid phase by vacuum filtration and washed with demineralized water. The solids were dried at 80 °C for 24 h, calcined at 550 °C for 6 h, and weighed before characterization.

2.3. Postsynthesis Alkaline Treatment of Products. In order to dissolve the silicalite-1 core of the product particles (silicalite-1/ZSM-5 composite particles), and thus to obtain hollow ZSM-5 particles, selected samples of the calcined crystalline end products were treated by hot alkaline (sodium carbonate) solution. Then, 0.5 g of each of the calcined samples was suspended in 15 mL of 0.8 M sodium carbonate solution. The suspensions were heated at 80 °C for 36 h under stirring and thereafter filtered to separate the solid (alkaline-treated ZSM-5) from the liquid phase. The solid samples were washed by demineralized water and dried at 100 °C for 24 h. The filtrate was also collected and used for determination of the concentrations of silicon and aluminum in the liquid phase.

2.4. Characterization. Scanning electron microscopy (SEM) measurements were performed by a Philips XL30 D6716 instrument at an operating voltage of 25 kV. Transmission electron microscopy (TEM) images were made on a JEOL JEM-2010 instrument at an operating voltage of 200 kV. Silicon and aluminum contents in the liquid phase of the alkaline-treated mixture were determined by atomic absorption spectroscopy (AAnalyst 200, Perkin-Elmer) and used for calculation of dissolved amount (mass fraction) of the alkaline treated products. X-ray diffraction (XRD) patterns were recorded on a Rigaku D/Max-rB 12 kW diffractometer (Cu K_α). Crystallinity, C_M (in %),

dx.doi.org/10.1021/cg200981d | Cryst. Growth Des. 2012, 12, 1736–1745

and fraction, $f_c(M) = C_M/100$, respectively, of the crystalline phase in the solid samples, separated from the reaction mixtures at different crystallization times, t_c, was calculated by the Hermans–Weidinger method.[16] Briefly, a series of the standard samples with defined crystallinities, C_S, from 10% to 90% were prepared by mixing and homogenization of fully amorphous phase (fresh gel) and fully crystalline product. XRD patterns of the standard samples as well as of the samples separated from the reaction mixtures at different crystallization times, t_c, were normalized in the 2θ range between 22.5° and 25°. Then, the value of a_T, which equals the sum of the surface areas of peaks (a_p) and the surface area of the amorphous "maximum" above the baseline (a_a) in the same range were calculated for all the samples. For given values of $a_T(M)$, which correspond to the samples separated from the reaction mixtures at different crystallization times, t_c, the corresponding values of C_M were determined from the linear relationship between C_S and $a_T(S)$, which correspond to standard samples.

Particles (crystals) size distribution (PSD) curves of the used seed crystals as well as of the products of hydrothermal and/or postsynthesis alkaline treatments were determined with a Malvern Mastersizer 2000 laser light-scattering (LLS) particle size analyzer. Then, using the PSD data, the average crystal size, D_{av}, and specific number of crystals, N_S (number of crystals per one gram of the seed crystals) were calculated as[17]

$$D_{av} = \sum N_j \times D_j / \sum N_j \quad (1)$$

$$N_S = \sum N_j/(\pi/6) \times \rho \times \sum N_j \times (D_j)^3 \quad (2)$$

where N_j is the number frequency of the crystals having the size between D and δD, $D_j = D + \delta D/2$, D is measured equivalent spherical diameter, and $\rho = 1.8$ g/cm^3 is the density of silicalite-1.

3. POPULATION BALANCE METHODOLOGY AND PRINCIPLES OF SIMULATION

Previous investigation has shown that in the absence of seed crystals, a nonporous XRD amorphous product was obtained after hydrothermal treatment (at 210 °C for 2 h) of the reaction mixture: $1.0Al_2O_3/100SiO_2/28Na_2O/4000H_2O$ (see Figure 4 in ref 13). The absence of crystalline phase indicates that nuclei did not form (and growth) during the reaction time (about 2 h) relevant for the entire transformation of the amorphous phase (gel) into crystalline one (zeolite ZSM-5) in the seeded reaction mixtures.[13] On the other hand, there are abundant data on the influence of seed crystals on zeolite crystallization.[2b,10,11,18] Although the primary effects/purposes of seeding are (i) shortening or even "elimination" of the "induction period", (ii) increasing of the overall rate of crystallization, and (iii) controlling of the product crystal size; there is much evidence that the addition of seed crystals into reaction mixture considerably reduces or even entirely eliminates the nucleation processes.[18]

Now, on the basis of the previous knowledge and experience in modeling and simulation of zeolite crystallization processes[19] and taking into consideration that new nuclei are not formed in the presence of seed crystals, the population balance of the SDA-free crystallization process can be defined as

$$d(m_o)_j/dt_c = dN/dt_c = 0 \quad (3)$$

$$d(m_1)_j/dt_c = Q \times (m_o)_j \quad (4)$$

$$d(m_2)_j/dt_c = 2 \times Q \times (m_1)_j \quad (5)$$

$$d(m_3)_j/dt_c = 3 \times Q \times (m_2)_j \quad (6)$$

$$Q = d(\Delta D)/dt_c \quad (7)$$

where $(m_i)_j = \int (D_j)^i (dN_j/dD_j) dD_j$ is ith (i = 0, 1, 2, and 3) moment of the particle size distribution of zeolite crystals at crystallization time t_c, N_j is the number of crystals with size D_j at the crystallization time t_c and Q is the rate of crystal growth, that is, increase of the size, ΔD of seed crystals during crystallization. The subscript j represents particular populations of the crystals having the size among 20 nm increments, that is, δD = 20 nm (see Supporting Information). Since the zeroth moment of particle size distribution represents the change in the number of particles (kinetics of nucleation), its value is zero (see eq 3) in the absence of nucleation process.

Previous kinetic analysis of the investigated systems[13] have shown that the added seed crystals grew with the constant rate, $d(\Delta D)/dt_c = K_g = 1.5 \times 10^{-5}$ cm/h and that the growth rate does not depend either on the size or amount of the seed crystals added in the reaction mixture. Now, knowing that measured fractions, f_c, of crystalline phase (zeolite ZSM-5) continuously increase, with increasing rate, until the end of crystallization process ($t_c = t_c$(end); see Figure 5 in ref 13), it is reasonable to conclude that the growth rate is constant to $t_c = t_c$(end) when ΔD reaches its maximum value, that is,

$$\Delta D_{max} = K_g \times t_c(\text{end}) \quad (8)$$

This results in typical growth functions (see Figure 1) characteristic for many crystallization kinetics of MFI-type zeolites.[20,21]

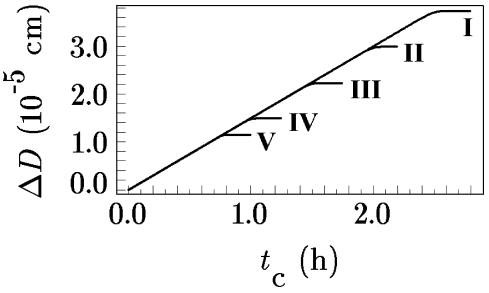

Figure 1. Change of the increase, ΔD, of crystal size, calculated by the solution of eq 5 using $K_g = 1.5 \times 10^{-5}$ cm/h and the corresponding values of K_d and ΔD_{max} listed in Table 1, during crystallization of zeolite ZSM-5 in systems S690-4 (I), S260-4 (II), S260-8 (III), S260-16 (IV), and S260-32 (V).

On the basis of previous analyses of many kinetics of crystal growth of zeolites, it was found that the typical profile of zeolite growth rate curves[20] can be satisfactorily fitted by a solution of the differential equation,[19c,20]

$$Q = d(\Delta D)/dt_c = K_g \times \{1 - \exp[K_d \times (\Delta D - \Delta D_{max})]\} \quad (9)$$

where K_d is the factor which determines the deviation of the ΔD vs t_c function from linearity (see Figure 1). Using known values of $K_g = 1.5 \times 10^{-5}$ cm/h and ΔD_{max} calculated by eq 8 (see Table 1), the corresponding values of K_d (see Table 1) were determined (calculated) by iterative solution of eq 8, that is, by finding out the value of K_d which fits the ΔD vs t_c function in a satisfactory way.

Thus, the changes in the mass, m_z, and incremental sizes, $(D_p)_j$, of zeolite ZSM-5 formed during the crystallization process were simulated (calculated) by simultaneous solution

Table 1. Numerical Values of the Maximum Increase, ΔD_{max}, of Crystal Size and of the Factor, K_d, Which Correspond to Systems S690-4, S260-4, S260-8, S260-16, and S260-32

system	S690-4	S260-4	S260-8	S260-16	S260-32
ΔD_{max} (cm)	3.75×10^{-5}	3.0×10^{-5}	2.24×10^{-5}	1.5×10^{-5}	1.16×10^{-5}
K_d	2.0×10^{6}	2.5×10^{6}	3.0×10^{6}	4.0×10^{6}	5.0×10^{6}

of differential eqs 3−6 and 9 by the fourth-order Runge−Kuta method using the corresponding values of constants (input data) and initial conditions.

3.1. Input Data (Constants). Growth rate constant: $K_g = 1.5 \times 10^{-5}$ cm/h, for all systems.

Specific number of seed crystals: $N_s = 3.08 \times 10^{12}$ crystals/g for seed s-690 (system S690-4) and $N_s = 4.1 \times 10^{13}$ crystals/g for seed s-260 (systems S260-4, S260-8, S260-16, and S260-32).

3.2. Initial Conditions.

$$(m_o)_j(t_c = 0) = (N_s)_j \times [(D_s)_j]^0 = (N_s)_j$$

$$(m_1)_j(t_c = 0) = (N_s)_j \times [(D_s)_j]^1 = (N_s)_j \times (D_s)_j$$

$$(m_2)_j(t_c = 0) = (N_s)_j \times [(D_s)_j]^2$$

$$(m_3)_j(t_c = 0) = (N_s)_j \times [(D_s)_j]^3$$

$$\Delta D(t_c = 0) = 0$$

Here, $(N_s)_j$ is the incremental number of seed crystals having the size between $(D_s)_j - 1 \times 10^{-6}$ cm and $(D_s)_j + 1 \times 10^{-6}$ cm. The values of $(N_s)_j$ and $(D_s)_j$ were determined by the appropriate PSDs of the seed crystals (Figure 2) and listed in Table S1 (see Supporting Information).

3.3. Output Data (Results). The values of ΔD at different crystallization times, t_c, were obtained in a direct way by the appropriate solution of eqs 7 and 9, respectively, that is,

$$\Delta D = \int Q \, dt_c = K_g \times \int \{1 - \exp[K_d \times (\Delta D - \Delta D_{max})]\} \, dt_c$$

Then, the changes in the incremental sizes, $(D_p)_j$, of product particles (crystals) were calculated as

$$(D_p)_j = (D_s)_j + \Delta D = (D_s)_j + \int Q \, dt_c = (D_s)_j + K_g \times \int \{1 - \exp[K_d \times (\Delta D - \Delta D_{max})]\} \, dt_c$$

Finally, since the value of the third moment of particle size distribution is proportional to the volume of given particles population, that is, $(m_3)_j = (N_p)_j \times [(D_s)_j]^3$, the incremental mass of product, $(m_z)_j$, is

$$(m_z)_j = G \times \rho \times (N_p)_j \times [(D_s)_j]^3 = G \times \rho \times (m_3)_j = 3 \times G \times \rho \times \int Q \times (m_2)_j \, dt_c$$

and thus, the overall mass, m_z, of the product crystallized at time t_c is calculated as

$$m_z = 3 \times G \times \rho \times \sum [\int Q \times (m_2)_j \, dt_c]$$

where $G = \pi/6$ (geometrical shape factor) and $\rho = 1.8$ g/cm^3 (density of the MFI-type zeolites).

4. RESULTS AND DISCUSSION

From the SEM images of the crystalline end products, obtained by hydrothermal treatment of the systems S690-4, S260-4, S260-8, S260-16, and S260-32 (see Figure 3), it is easy to find

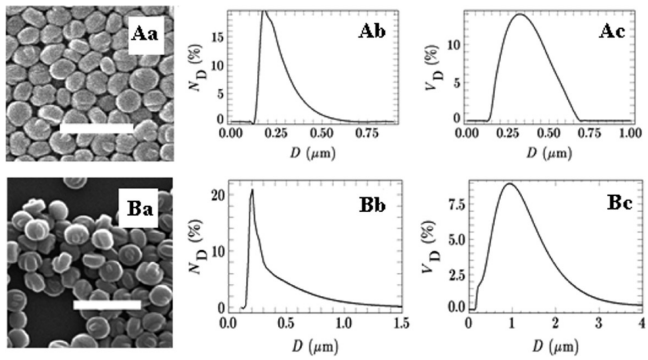

Figure 2. SEM images (Aa, Ba) and particle size distributions by number (Ab, Bb) and volume (Ac, Bc) of silicalite-1 seed crystals s-260 (A) and s-690 (B). N_D is the number percentage and V_D is the volume percentage, respectively, of crystals having the spherical equivalent diameter D. Scale bars: 1 μm in panel Aa; 2 μm in panel Ba.

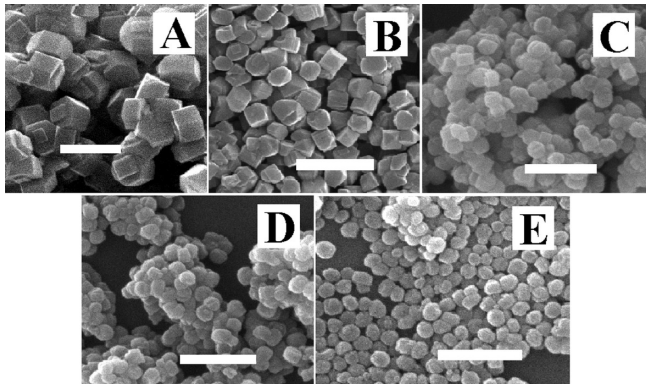

Figure 3. SEM images of the crystalline end products obtained by hydrothermal treatment of the systems S690-4 (A), S260-4 (B), S260-8 (C), S260-16 (D), and S260-32 (E). The scale bars in all panels represent 2 μm.

out that the size ranges of individual crystals for a given system correspond to these calculated by the simple relationship,

$$(D_p)_j = (D_s)_j + \Delta D_{max} \quad (10)$$

Thus, it indicates the validity of the values of ΔD_{max} calculated, by eq 8, as shown in Figure 1. Here it must be emphasized that

dx.doi.org/10.1021/cg200981d | Cryst. Growth Des. 2012, 12, 1736−1745

the values of ΔD_{max} calculated by eq 8 are in excellent agreement with the values of ΔD_{max} determined from the corresponding SEM images.[13]

Figure 4A–4E shows the measured absolute crystal size distributions $[(N_s)_j$ vs $(D_s)_j]$ of the used amounts of silicalite-1

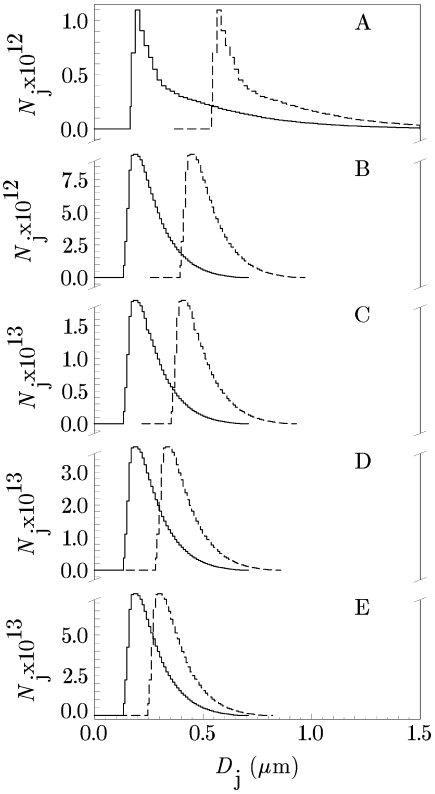

Figure 4. Solid curves; measured PSDs of silicalte-1 seeds s-690 (A) and s-260-4 (B–E), presented as the number, $N_j = (N_s)_j$, of crystals having the incremental size $D_j = (D_s)_j$. Dashed curves: simulated (calculated) PSDs of the crystalline end products in systems S690-4 (A), S260-4 (B), S260-8 (C), S260-16 (D), and S260-32 (E), presented as the number $N_j = (N_p)_j$, of crystals having the incremental size $D_j = (D_p)_j$.

seed crystals (solid curves) and the calculated (simulated) absolute crystal size distributions $[(N_p)_j$ vs $(D_p)_j]$ of the products (zeolite ZSM-5; dashed curves) formed by crystal growth of the silicalite-1 seed crystals. Very good agreements between measured and calculated (simulated) sizes of the smallest particles (PSDs of the products in Figure 5) firmly indicate that the smallest product particles are formed by the growth of the smallest seed crystals. In the case of the formation of additional nuclei, the particles smaller than these calculated on the basis of the model would appear in the crystalline end products. As expected from the SEM images in Figure 3, for a constant amount of seed crystals, the overall crystal size of the products increases with increasing overall crystal size of seed crystals, while the overall crystal size of the products decreases with increasing amounts of used seed crystals of the same size (see Figures 4 and 5). On the other hand, while the measured and calculated (simulated) PSD curves of the products are the same for system S260-32 (Figure 5E), almost the same for system S-260-16 (see Figure 5D), or in a fair agreement for system S690–4 (Figure 5A), there is a considerable disagreement between measured and calculated (simulated) PSD curves for $D > 0.5$ μm in systems S260-4

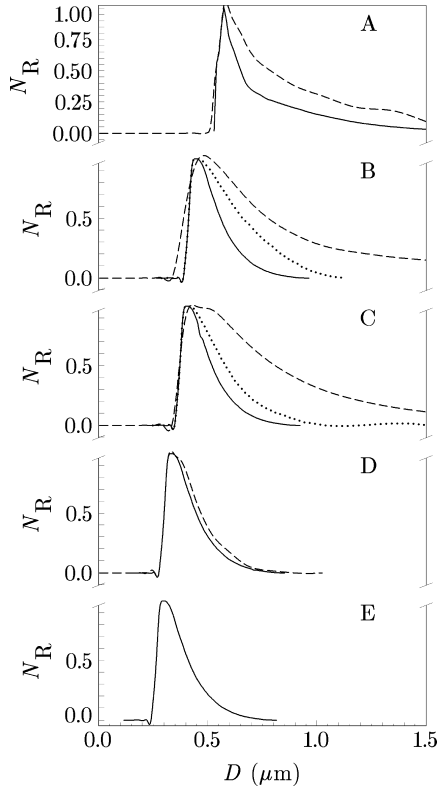

Figure 5. Calculated (solid curves) and measured (dashed curves) relative PSDs of the crystalline end products in systems S690-4 (A), S260-4 (B), S260-8 (C), S260-16 (D), and S260-32 (E). Dotted curves in panels B and C represent the PSDs of alkaline-treated products. $N_R = (N_d)_j/[(N_d)_j]_{max}$, where $[(N_d)_j]_{max}$ is the maximum (peak) value of (N_d), that is, $(N_d)_j = (N_d)_{peak}$.

(Figure 5B) and S260-8 (Figure 5C). This disagreement can be simply explained by the formation of a small fraction of crystal aggregates during the crystallization.[22] The approaching of the measured PSD curves of alkaline treated products (dotted curves in Figure 5B,C) to the calculated PSD curves confirms such an explanation. Namely, following the finding that tetrahedral aluminum centers are relatively inert to hydroxide attack due to the negative charges associated with these centers,[23] it is evident that alkaline treatment of the products (see Experimental Section) does not cause dissolution of aluminosilicate surface of crystals, but only more siliceous crystal "core"[13,15] and deaggregation, without the decrease in the size of the single, previously aggregated crystals.[13] However, at present, it is not quite clear why the larger crystals of the final products obtained in systems S690-4, S260-4, and S260-8 have a more expressive tendency to make aggregates than the smaller crystals obtained in systems S260-16 and S260-32.

Figure 6A–E shows the calculated (simulated) changes (increase) of the mass, m_z, of zeolite ZSM-5 crystallized in 100 g of the reaction mixture of investigated systems. The changes in the amounts of crystallized MFI-type zeolite (silicalite-1 seed crystals + crystallized zeolite ZSM-5) are calculated by simultaneous solution of differential eqs 3–6 and 9. Then, the value of m_z is expressed as explained in "Output data". On the other hand, Figure 7A–E shows the simulated changes (decrease) of the mass, m_G, of remaining (untransformed) amorphous phase (gel) in 100 g of examined reaction mixtures,

dx.doi.org/10.1021/cg200981d | Cryst. Growth Des. 2012, 12, 1736–1745

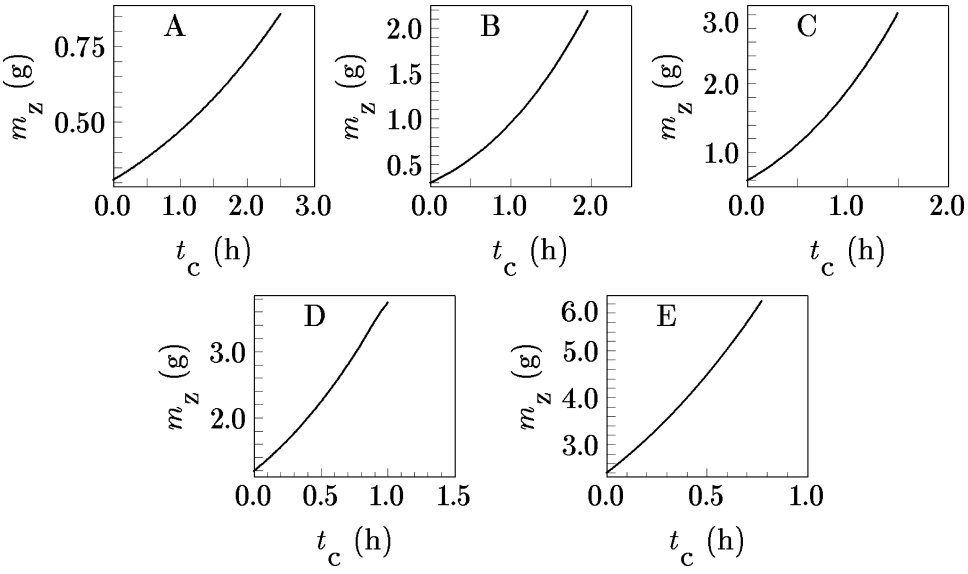

Figure 6. Calculated (simulated) changes of mass, m_z, of zeolite ZSM-5 crystallized from 100 g of the reaction mixture in systems S690-4 (A), S260-4 (B), S260-8 (C), S260-16 (D), and S260-32 (E). t_c is the time of crystallization.

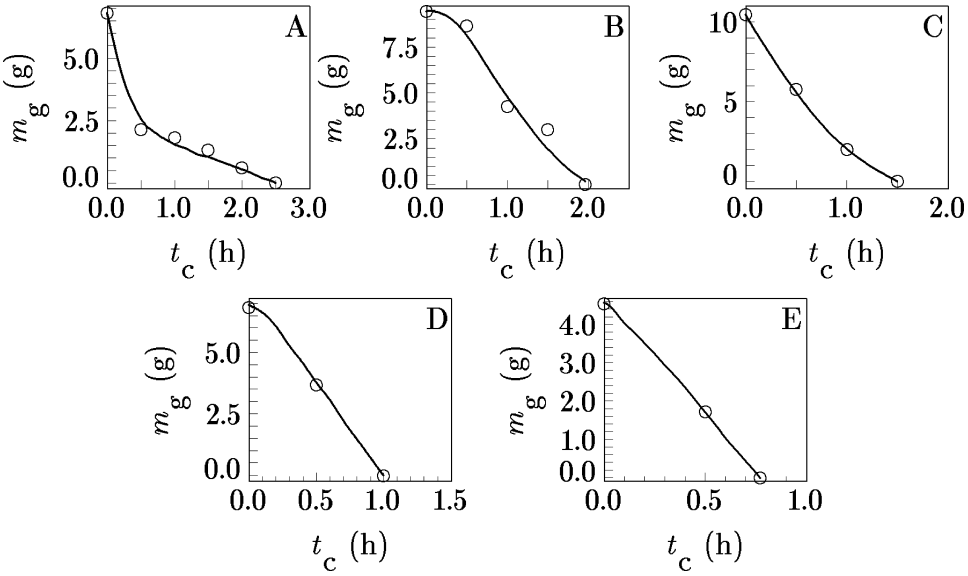

Figure 7. Changes of the mass, m_G, of the untransformed amorphous phase in 100 g of the reaction mixture in systems S690-4 (A), S260-4 (B), S260-8 (C), S260-16 (D), and S260-32 (E). t_c is the time of crystallization.

during their hydrothermal treatment. The mass, m_G, was calculated as

$$m_G = [1 - f_c(M)] \times m_s \quad (11)$$

where m_s is the mass of the solid phase (silicalite-1 seed crystals + crystallized zeolite ZSM-5 + remaining amorphous phase) separated from 100 g of reaction mixture at crystallization time, t_c, and $f_c(M)$ is the fraction of crystalline phase (silicalite-1 seed crystals + crystallized zeolite ZSM-5), determined from the corresponding XRD patterns of the solid phase separated from the reaction mixture at crystallization time t_c (see Experimental section).

Then, the change of the fractions, $f_c(C)$, of crystalline phase during seed-induced, TPA-free crystallization of zeolite ZSM-5 can be calculated as

$$f_c(C) = m_z/[m_z + m_G(f)] \quad (12)$$

where the values of $m_G(f)$ (curves in Figure 7A–E) represent the best fits of the corresponding m_G vs t_c functions, calculated by eq 11.

Very good or almost perfect correlations between measured [$(f_c(M)$; points in Figure 8)] and calculated [$f_c(C)$; curves in Figure 8] changes of the fractions of crystallized zeolite ZSM-5 as well as satisfactory agreement between calculated and measured PSDs of the crystalline end products (Figure 5), in a wide range of sizes and amounts, respectively, of added seed crystals show that the SDA-free process of crystallization takes place in accordance with the proposed model, that is, by a linear, size-independent growth of seed crystals. Thus, the process of crystallization is consistent with the process of crystallization occurring in the absence of extra nucleation.[13,22] The agreements between the measured and calculated (simulated) data also show that formation of aggregates does not considerably influence the growth rate of zeolite ZSM-5 on

dx.doi.org/10.1021/cg200981d | Cryst. Growth Des. 2012, 12, 1736–1745

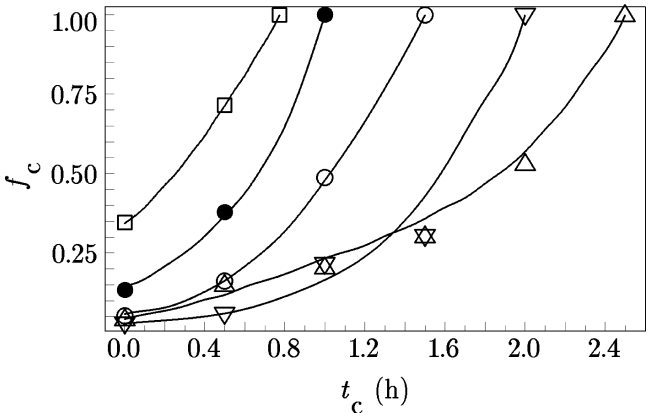

Figure 8. Simulated ($f_c = f_c$(C); curves) and measured ($f_c = f_c$(M); points) changes of the fraction f_c of zeolite ZSM-5 crystallized during hydrothermal treatment of the reaction mixtures (systems) S690-4 (△), S260-4 (▽), S260-8 (○), S260-16 (●), and S260-32 (□). t_c is the time of crystallization.

silicalite-1 seed crystals. This is in accordance with finding that the seed crystals are embedded in the gel matrix and thus that there is not close contacts between growing seed crystals during the main part of the crystallization process.[13] In this context, it is reasonable to conclude that the formation of crystal aggregates takes place at the end of crystallization process, that is, when the entire amount of amorphous phase (gel) has been transformed into zeolite ZSM-5.

As already reported in our previous work,[13] a postsynthesis alkaline treatment of the crystalline end products results in the formation of fully crystalline hollow particles of zeolite ZSM-5 (see Figures 9−11 and scheme in Figure 12), by the already

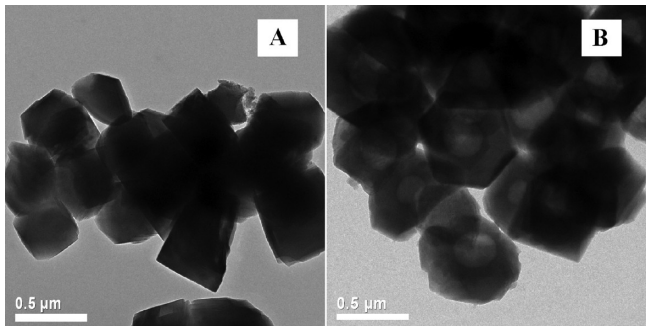

Figure 9. TEM images of the crystalline end products obtained by hydrothermal treatment of system S260-4 before (A) and after alkaline treatment (B). The scale bars in both figures represent 500 nm.

explained reason. The mass fractions, $(f_d)_{meas}$, of the material dissolved during alkaline treatment is determined (calculated) as

$$(f_d)_{meas} = (m_d)_{meas}/(m_p)_a = V_a \times C_{Si} \times (M_{sil}/M_{Si})/(m_p)_a = 64.18 \times C_{Si} \quad (13)$$

where $(m_d)_{meas}$ is the measured mass of material dissolved during alkaline treatment, $(m_p)_a$ = 0.5 g is the mass of alkaline treated crystalline end products (see Experimental Section), V_a = 15 mL is the volume of 0.8 M sodium carbonate solution used for alkaline treatment of the crystalline end products (see

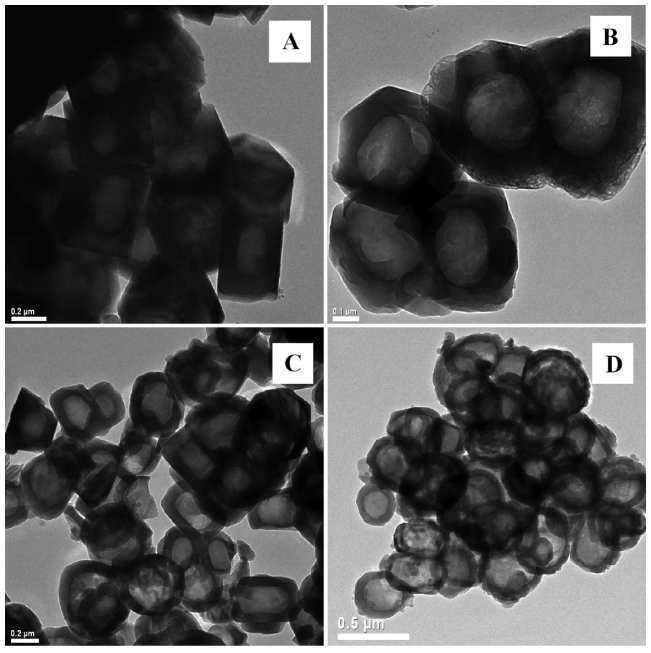

Figure 10. TEM images of the alkaline-treated products obtained by hydrothermal treatment of systems S260-4 (A), S-260-8 (B), S260-16 (C), and S260-32 (D). The scale bar represents 200, 100, 200, and 500 nm from A to D, respectively.

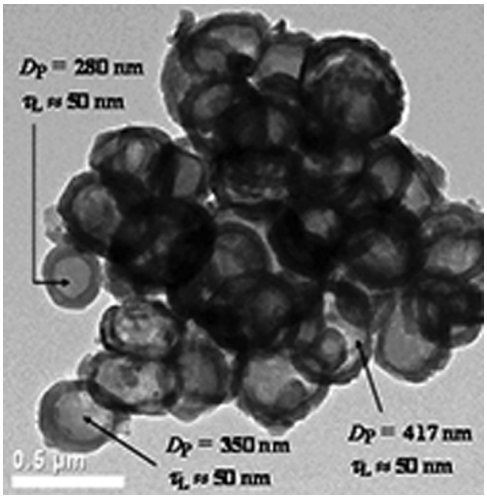

Figure 11. TEM image of the alkaline-treated product obtained by hydrothermal treatment of system S260-32. D_p is the size (diameter) of alkaline-treated product particles, and τ_L is the thickness of shell (layer); see also the scheme in Figure 12.

Experimental Section), M_{sil} = 60.084 is the molecular weight of SiO_2, M_{Si} = 28.086 is the atomic weight of silicon, and C_{Si} (in g/mL) is the concentration of silicon in the solution after alkaline treatment. On the other hand, by measuring the size, D_p, of the product particles and thickness, τ_L, of shell (layer) of particles in a large number of TEM images (see, for example, Figure 11) and analyzing the relationship between D_p, τ_L, D_s, and ΔD_{max} (see scheme in Figure 12) it can be concluded that (i) For a given system, determined by the size and amount of added silicalite-1 seed, the thickness, τ_L, of shell (layer) is proportional to ΔD_{max}, that is,

$$\tau_L \approx 0.4 \times \Delta D_{max} \quad (14)$$

dx.doi.org/10.1021/cg200981d | Cryst. Growth Des. 2012, 12, 1736−1745

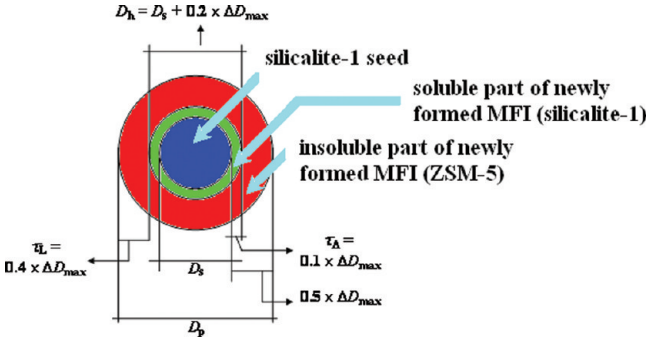

Figure 12. Schematic presentation of the relationships between size, D_s, of seed, thickness, τ_Δ, of the dissolved layer of crystallized phase, size, D_h, of the hole formed by dissolution of seed and a part of crystallized phase, thickness, τ_L, of the undissolved layer, ΔD_{max} and size, D_p, of product particle.

and thus, does not depend on the size, $(D_p)_j$ of individual product particles (see Figure 11). (ii) $(D_h)_j$ (size of the hole formed by dissolution of the "cores" of individual product particles during alkaline treatment) can be expressed as (see Figure 12)

$$(D_h)_j = (D_p)_j\text{-}2 \times \tau_L = (D_p)_j - 0.8 \times \Delta D_{max} \quad (15)$$

Now, combining eqs 10 and 15 gives

$$(D_h)_j = (D_s)_j + 0.2 \times \Delta D_{max} = (D_s)_j + 2 \times \tau_\Delta \quad (16)$$

This indicates that not only silicalite-1 seed but also a part of new formed MFI was dissolved during alkaline treatment, that is, $(D_h)_j > D_p - D_s$ (see eqs 15 and 16), where $\tau_\Delta = 0.1 \times \Delta D_{max} = 0.25 \times \tau_L$ is the thickness of the layer of dissolved part of new formed MFI (see scheme in Figure 12). Thus, the mass, m_d, of the material dissolved during alkaline treatment can be expressed as

$$m_d = G_1 \times \rho \times \sum (N_s)_j \times [(D_h)_j]^3 = G_1 \times \rho \times \sum (N_s)_j \times [(D_s)_j + 0.2 \times \Delta D_{max}]^3 \quad (17)$$

where $G_1 = \pi/6$ is volume shape factor of the seed crystals having equivalent spherical diameters $(D_p)_j$. Consequently, the mass fraction, f_d, of the material dissolved during alkaline treatment can be calculated as

$$(f_d)_{calc} = m_d/m_p = \sum \{[(D_s)_j + 0.2 \times \Delta D_{max}]/[(D_s)_j + \Delta D_{max}]\}^3 \quad (18)$$

where, in accordance with eq 10,

$$m_p = G_1 \times \rho \times \sum (N_s)_j \times [(D_p)_j]^3 = G_1 \times \rho \times \sum (N_s)_j \times [(D_s)_j + \Delta D_{max}]^3 \quad (19)$$

Using the corresponding PSD curves [$(N_s)_j$ vs $(D_p)_j$ functions] of seed crystals and the corresponding values of ΔD_{max} (see Figure 1 and Table 1), the fractions, $(f_d)_{calc}$, are calculated by eq 18. These data are compared with the fractions, $(f_d)_{meas}$, calculated by eq 13, using the measured values of C_{Si} (see Experimental Section) in Table 2.

Satisfactory or even good agreement between measured and calculated fractions of the material dissolved during the

Table 2. Calculated, $(f_d)_{calc}$, and Measured, $(f_d)_{meas}$ Mass Fractions of Material (Silica) Dissolved during Alkaline Treatment of the Crystalline End Products Obtained from Systems S690-4, S260-4, S260-8, S260-16, and S260-32

system	S690-4	S260-8	S260-16	S260-32
$(f_d)_{calc}$	0.446	0.294	0.409	0.487
$(f_d)_{meas}$	0.467	0.321	0.434	0.502

postsynthesis alkaline treatments of the crystalline end products (Table 2) undoubtedly proves the validity of the relationships between τ_Δ, τ_L, D_s, D_h, ΔD_{max}, and D_p expressed by eqs 10 and 14−19 as schematically presented in Figure 12. Somewhat higher values of $(f_d)_{meas}$ relative to the values of $(f_d)_{calc}$ (from about 3% for system S260-32 to about 9% for system S260-8; see Table 2) are probably caused by the fact that both the product particles and holes are not perfect spheres used for calculation of $(f_d)_{calc}$ and/or possible partial (slight) desilication of the surface/subsurface layer of the product particles.

Dissolution of a part of MFI, formed by starting growth of silicalite-1 seeds, leads to a reasonable assumption that the dissolved part of newly formed crystalline phase represents Al-free MFI (silicalite-1) rather than zeolite ZSM-5. The absence of Al in the liquid phase (filtrate) obtained after alkaline treatment (see also ref 13) supports such an assumption. This is also in accordance with the finding that "...the initial crystallization proceeds towards the formation of silicalite-like phase, where the aluminum is inside the solid, but not inside the crystalline lattice."[24] Thus, by abundant evidence that aluminum is invariably concentrated in the rim portion of the crystals of zeolite ZSM-5.[24,25]

Now, following the relationships between τ_Δ, τ_L, D_s, D_h, ΔD_{max}, and D_p expressed by eqs 10 and 14−19 and schematically represented in Figure 12 and using the appropriate $(N_s)_j$ vs $(D_s)_j$ and $(N_p)_j$ vs $(D_p)_j$ functions (Figure 4A−E), the corresponding geometrical surface areas of the products before and after alkaline treatment can be calculated by the following relations:

$$A_p(tot) = \pi \times \sum (N_p)_j \times [(D_p)_j]^2 = \pi \times \sum (N_s)_j \times [(D_s)_j + \Delta D_{max}]^2 \quad (20)$$

$$A_p(sp) = A_p(tot)/m_p \quad (21)$$

$$A_{at}(tot) = \pi \times \sum (N_p)_j \times [(D_p)_j]^2 + \pi \times \sum (N_p)_j \times [(D_h)_j]^2 = \pi \times \sum \{(N_s)_j \times [(D_s)_j + \Delta D_{max}]^2 + (N_s)_j \times [(D_s)_j + 0.2 \times \Delta D_{max}]^2\} \quad (22)$$

$$A_{at}(sp) = A_{at}(tot)/m_{at} \quad (23)$$

Here, $A_p(tot)$ and $A_{at}(tot)$ are the total geometrical surface areas before and after alkaline treatment, $A_p(sp)$ and $A_{at}(sp)$ are the specific geometrical surface areas before and after alkaline treatment, and

$$m_{at} = m_p - m_d \quad (24)$$

is the mass of product remained undissolved after alkaline treatment, where m_p is the mass of product before alkaline

dx.doi.org/10.1021/cg200981d | Cryst. Growth Des. 2012, 12, 1736−1745

treatment, as defined by eq 19 and m_d is the mass of material dissolved during alkaline treatment, as defined by eq 17.

The results in Table 3 show that, as expected, both $A_p(sp)$ and $A_{at}(sp)$ increase with a decrease of particle (crystal) size of

Table 3. Values of ΔD_{max} as well as the Total, $A(tot)$ and Specific, $A(sp)$, Geometrical Surface Areas of the Products before $[A(tot) = A_p(tot); A(sp) = A_p(sp)]$ and after Alkaline Treatment $[A(tot) = A_{at}(tot); A(sp) = A_{at}(sp)]$ and Their Ratios $A_{at}(tot)/A_p(tot)$ and $A_{at}(sp)/A_p(sp)$, Which Correspond to 100 g of Systems S690-4, S260-4, S260-8, S260-16, and S260-32

system	S690-4	S260-4	S260-8	S260-16	S260-32
ΔD_{max} (μm)	0.375	0.300	0.225	0.150	0.116
$A_p(tot)$ (m^2)	32.08	168.05	253.80	370.16	629.12
$A_p(sp)$ (m^2/g)	2.81	5.60	6.35	7.29	7.80
$A_{at}(tot)$ (m^2)	47.99	226.41	360.60	565.38	1003.22
$A_{at}(sp)$ (m^2/g)	7.59	9.68	12.79	18.85	24.23
$A_{at}(tot)/A_p(tot)$	1.50	1.35	1.42	1.53	1.60
$A_{at}(sp)/A_p(sp)$	2.70	1.73	2.01	2.59	3.11

product and with simultaneous increase of ΔD_{max}. Although it is reasonable to expect that the total geometrical surface area, $A_{at}(tot) = A_{at}(sp) \times m_{at}$, can be maximally two times higher than the total geometrical surface area $A_p(tot) = A_p(sp) \times m_p$, that is, $A_{at}(tot)/A_p(tot) \rightarrow 2$ when $\tau_L \rightarrow 0$, the data in Table 3 show that for most of the products, this ratio is around 1.5. However, a more profound increase of the geometrical specific surface area after alkaline treatment is observed, for example, $A_{at}(sp)/A_p(sp) = 2.7$ for system S690-4 and even 3.11 for system S260-32. The values $A_{at}(sp)/A_p(sp) > 2$ are the consequence of the decrease in the mass of alkaline treated sample ($m_{at} < m_p$), caused by partial dissolution of crystal "core" during the treatment.[13] Figure 13 shows that both the

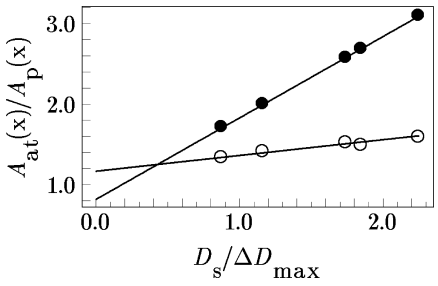

Figure 13. $A_{at}(tot)/A_p(tot)$ vs $D_s/\Delta D_{max}$ (x = tot; ○) and $A_{at}(sp)/A_p(sp)$ vs $D_s/\Delta D_{max}$ (x = sp; ●) plots.

ratios, $A_{at}(tot)/A_p(tot)$ and $A_{at}(sp)/A_p(sp)$ are linear functions of the ratio $D_s/\Delta D_{max}$, that is,

$$A_{at}(tot)/A_p(tot) = 1.17 + 0.195 \times D_s/\Delta D_{max} \quad (25)$$

and

$$A_{at}(sp)/A_p(sp) = 0.82 + 1.01 \times D_s/\Delta D_{max} \quad (26)$$

Although eqs 25 and 26 represent empirical relationships which do not include the value of N_s (which also influence the value of ΔD_{max}), they generally show the trends of the impact of postsynthesis alkaline treatment on the change (increase) of surface area. At the same time, the relationships presented by eqs 25 and 26 are a good basis for further development of the exact relationships between surface area of alkaline treated products and the related parameters (D_s, N_s, composition of the reaction mixture), which could make great contributions for the studies of high-silica zeolites with Al-zoning distributions in the framework.

5. CONCLUSION

By population balance analysis of the crystallization of zeolite ZSM-5 from TPA-free reaction mixture in the presence of silicalite-1 seed crystals, it has been revealed that

- The crystallization process takes place by a linear, size-independent growth of the seed crystals embedded in the gel matrix, as proved by very good or almost excellent agreement between calculated (simulated) and measured kinetics of crystallization (f_c vs t_c functions). This indicates that the process of crystallization is consistent with the absence of extra nucleation in the presence of seeds crystals.
- The particulate properties (particle size distribution) of the crystalline end products can also be successfully simulated in the frame of the appropriate model. The satisfactory correlations between measured and simulated data are observed for $D_p < 0.5$ μm. Small disagreement between measured and simulated data for $D_p \geq 0.5$ μm can be explained by the formation of a small proportion of crystal aggregates during crystallization.
- For the alkaline-treated samples, the ratio, $\tau_L/\Delta D_{max} \approx 0.4$ (τ_L is the thickness of the layer of hollow particles obtained by alkaline treatment of product and ΔD_{max} is the maximum increase of particles size caused by growth of seeds) does not depend either on the number/size of added seed crystals or on the size, D_p, of the product obtained in a given system.
- Although the crystallization of zeolite ZSM-5 from a SDA-free system can be successfully and in short time (about 2 h) realized with a small amount (e.g., 4 wt %) of seed crystals, the increase of the amount of seed crystals (even in an "non-standard" extent, e.g., 32 wt %) is also favorable from both scientific and practical aspects, for example, increasing the eventually "active" surface or forming zeolitic microcapsules with ultrathin shells for advanced applications.
- The increase of geometrical surface area of samples after alkaline treatment is calculated and expressed by simple empirical relationships. Such a finding also predicts the formation of a new silicalite-1 layer prior to the growth of ZSM-5 on the surface of silicalite-1 seed crystals during the crystallization process.

The obtained results show that the population balance methodology can be successfully used for prediction of crystallization pathway and particulate properties of products before and after alkaline treatment and for determining the optimal conditions to obtain the products possessing the desired properties needed for specific application(s).

■ ASSOCIATED CONTENT

Supporting Information

Detailed description of the analysis procedures of population balance methodology. This information is available free of charge via the Internet at http://pubs.acs.org/.

AUTHOR INFORMATION

Corresponding Author

*E-mail: subotic@irb.hr.

Notes

The authors declare no competing financial interest.

ACKNOWLEDGMENTS

This work is realized in the frame of the projects: NSFC (20803010), "Chen Guang" project supported by Shanghai Municipal Education Commission and Shanghai Education Development Foundation (09CG02), 'Brain Gain' Post-Doc project (I-668-2011) supported by National Foundation for Science, Higher Education, and Technological Development of the Republic of Croatia and project 098-0982904-2953, financially supported by the Ministry of Science, Education and Sport of the Republic of Croatia.

REFERENCES

(1) Baerlocher, C.; McCusker, L. B.; Olson, D. H. *Atlas of Zeolite Framework Types*, 6th revised ed.; Elsevier: Amsterdam, 2007.

(2) (a) Chang, C. D.; Silvestry, A. J. *J. Catal.* **1977**, *47*, 249−259. (b) Narita, E.; Sato, K.; Okabe, T. *Chem. Lett.* **1984**, 1055−1058. (c) Petrik, L. F.; O'Connor, C. T.; Schwartz, S. In *Proceedings of ZEOCAT'95*; Beyer, H. K., Karge, H. G., Kiricsi, I., Nagy, J. B., Eds.; Elsevier: Amsterdam, 1995; pp 517−524. (d) Kim, S. D.; Noh, S. H.; Park, J. W.; Kim, W. J. *Microporous Mesoporous Mater.* **2006**, *92*, 181−188.

(3) (a) Vanderpol, A. J. H. P.; Vanhooff, J. H. C. *Appl. Catal. A* **1993**, *106*, 97−113. (b) Weitkamp, J. *Solid State Ionics* **2000**, *131*, 175−188. (c) Panpranot, J.; Toophorm, U.; Praserthdam, P. *J. Porous Mater.* **2005**, *12*, 293−299.

(4) (a) Climent, M. J.; Corma, A.; Garcia, A.; Ibarra, M.; Prime, S. *J. Appl. Catal. A* **1995**, *130*, 5−12. (b) Loendres, R.; Jacobs, P. A.; Martens, J. A. *J. Catal.* **1998**, *176*, 545−551.

(5) (a) Firoozi, M.; Baghalha, M.; Asadi, M. *Catal. Commun.* **2009**, *10*, 1582−1585. (b) Jia, C. Y.; Liu, Y.; Schmidt, W.; Lu, A. H.; Schüth, F. *J. Catal.* **2010**, *269*, 71−79. (c) Wang, Y.; Guo, L. F.; Ling, Y.; Liu, Y. M.; Li, X. A. H.; Wu, H. H.; Wu, P. *Appl. Catal. A-Gen.* **2010**, *379*, 45−53.

(6) Coronas, J. *Chem. Eng. J.* **2010**, *156*, 236−242.

(7) (a) Chang, C. D.; Lang, W. H.; Silvestri, A. J. U.S. Patent 3,894,106, 1975. (b) Chang, C. D.; Silvestri, A. J.; Smith, R. L. U.S. Patent 3,928,483, 1975.

(8) Lai, R.; Gavalas, G. R. *Microporous Mesoporous Mater.* **2000**, *38*, 239−245.

(9) (a) Otake, M. *Zeolites* **1994**, *14*, 42−52. (b) Aiello, R.; Crea, F.; Nastro, A.; Pellegrino, A. *Zeolites* **1987**, *7*, 549−553. (c) Dai, F.-Y.; Suzuki, M.; Takahashi, H.; Saito, Y. *ACS Symp. Ser.* **1989**, *398*, 244−256. (d) Nastro, A.; Crea, F.; Hayhurst, D. T.; Testa, F.; Aiello, R.; Toniolo, L. *Stud. Surf. Sci. Catal.* **1989**, *49A*, 321−330.

(10) Batista, J.; Kaučič, V. *Vestn. Slov. Kem. Drus.* **1987**, *34*, 289−302.

(11) (a) Pan, M.; Lin, J. S. *Microporous Mesoporous Mater.* **2001**, *43*, 319−327. (b) Lassinatti, M.; Jereman, F.; Hedlund, J.; Creaser, D.; Sterte, J. *Catal. Today* **2001**, *67*, 109−119. (c) Narita, E.; Sato, K.; Yatabe, N.; Okabe, T. *Ind. Eng. Chem. Prod. Res. Dev.* **1985**, *24*, 507−512.

(12) (a) Lowe, B. M.; Nee, J. R. D.; Casci, J. L. *Zeolites* **1994**, *14*, 610−619. (b) Kalipcilar, H.; Culfaz, A. *Cryst. Res. Technol.* **2001**, *36*, 1197−1207.

(13) Ren, N.; Yang, Z.-J.; Lv, X.-C.; Shi, J.; Zhang, Y.-H.; Tang, Y. *Microporous Mesoporous Mater.* **2010**, *131*, 103−114.

(14) (a) Groen, J. C.; Moulijn, J. A.; Perez-Ramirez, J. *J. Mater. Chem.* **2006**, *16*, 2121−2131. (b) Perez-Ramirez, J.; Abello, S.; Bonilla, A.; Groen, J. C. *Adv. Funct. Mater.* **2009**, *19*, 164−172. (c) Mei, C. S.; Liu, Z. C.; Wen, P. Y.; Xie, Z. K.; Hua, W. M.; Gao, Z. *J. Mater. Chem.* **2008**, *18*, 3496−3500.

(15) Mei, C. S.; Wen, P. Y.; Liu, Z. C.; Liu, H. X.; Wang, Y. D.; Yang, W. M.; Xie, Z. K.; Hua, W. M.; Gao, Z. *J. Catal.* **2008**, *258*, 243−249.

(16) Hermans, P. H.; Weidinger, A. *Makromol. Chem.* **1961**, *44/46*, 24−37.

(17) Kolar, Z. I.; Binsma, J. J. M.; Subotić, B. *J. Cryst. Growth* **1992**, *116*, 473−482.

(18) (a) Culfaz, A.; Sand, L. B. *Adv. Chem. Ser.* **1973**, *121*, 140−151. (b) Kacirek, H.; Lechert, H. *J. Phys. Chem.* **1975**, *79*, 1589−1593. (c) Kacirek, H.; Lechert, H. *J. Phys. Chem.* **1976**, *80*, 1291−1296. (d) Dixon, A. G.; Thompson, R. W. *Zeolites* **1986**, *6*, 154−160. (e) Pittenger, B. H.; Thompson, R. W. *Zeolites* **1996**, *17*, 272−277. (f) Nikolakis, V.; Kokkoli, E.; Tirrell, M.; Tsapatsis, M.; Vlachos, D. G. *Chem. Mater.* **2000**, *12*, 845−853.

(19) (a) Thompson, R. W.; Dyer, A. *Zeolites* **1985**, *5*, 202−210. (b) Falamaki, C.; Edrissi, M.; Sohrabi, M. *Zeolites* **1997**, *19*, 2−5. (c) Bosnar, S.; Antonić, T.; Bronić, J.; Krznarić, I.; Subotić, B. *J. Cryst. Growth* **2004**, *267*, 270−282. (d) Creaser, D. *Stud. Surf. Sci. Catal.* **1999**, *25*, 117−124. (e) Provis, J. L.; Vlachos, D. G. *J. Phys. Chem B* **2006**, *110*, 3098−3108. (f) Aerts, A; Haouas, M; Caremans, T. P.; Follens, L. R. A.; van Erp, T. S.; Taulelle, F.; Vermant, J.; Martens, J. A.; Kirschhock, C. E. A. *Chem.—Eur. J.* **2010**, *16*, 2764−2774. (g) Lutsko, J. F.; Basios, V.; Nicolis, G.; Caremans, T. P.; Aerts, A.; Martens, J. A.; Kirschhock, C. E. A.; van Erp, T. S. *J. Chem. Phys.* **2010**, *132*, 64701.

(20) Subotić, B.; Bronić, J. In *Handbook of Zeolite Science and Technology*; Auerbach, S. M., Carrado, K. A., Dutta, P. K., Eds.; Marcel Dekker Inc.: New York, 2003; pp 129−203.

(21) (a) Twomey, T. A. M.; Mackay, M.; Kuipers, H. P. C. E.; Thompson, R. W. *Zeolites* **1994**, *14*, 162−168. (b) Persson, A. E.; Schoeman, B. J.; Sterte, J.; Otterstedt, J.-E. *Zeolites* **1995**, *15*, 611−619. (c) Watson, J. N.; Iton, L. E.; Keir, R. I.; Thomas, J. C.; Dowling, T. L.; White, J. W. *J. Phys. Chem. B* **1997**, *101*, 10094−10104. (d) de Moor, P.-P. E. A.; Beelen, T. P. M; van Santen, R. A. *J. Phys. Chem. B* **1999**, *103*, 1639−1650. (e) Hsu, C.-Y.; Chieng, A. S. T.; Selvin, R.; Thompson, R. W. *J. Phys. Chem. B* **2005**, *109*, 18804−18814.

(22) Ren, N.; Bronić, J.; Subotić, B.; Lv, X.-C.; Yang, Z.-J.; Tang, Y. *Microporous Mesoporous Mater.* **2011**, *139*, 197−206.

(23) (a) Iller, R. K. *The Chemistry of Silica*; Wiley: New York, NY, 1979. (b) Lechert, H.; Kacirek, H. *Zeolites* **1991**, *11*, 720−728. (c) Dessau, R. M.; Valyocsik, E. W.; Goeke, N. H. *Zeolites* **1992**, *12*, 776−779.

(24) Padovan, M.; Leofanti, G.; Solari, M.; Moretti, E. *Zeolites* **1984**, *4*, 295−299.

(25) (a) von Ballmoos, R.; Meier, W. M. *Nature* **1981**, *289*, 782−783. (b) Groen, J. C.; Bach, T.; Ziese, U.; van Donk, A. P. M; de Jong, K. P.; Moulijn, J. A.; Perez-Ramirez, J. *J. Am. Chem. Soc.* **2005**, *127*, 10792−10793. (c) Danilina, N.; Krumeich, F.; Castelanelli, S. A.; van Bokhoven, J. A. *J. Phys. Chem.* **2010**, *114*, 6640−6645.